High-pressure dc glow discharges in hollow diamond cathodes

High-pressure dc glow discharges in hollow diamond cathodes

B S Truscott, C Turner and P W May

School of Chemistry, University of Bristol, Bristol, BS8 1TS, UK

E-mail: Paul.May@bristol.ac.uk

CrossMark

Abstract

We report the generation and characterization of dc helium microdischarges at several times atmospheric pressure in monolithic diamond hollow-cathode devices having cavity diameters on the order of 100 μm. I–V characteristics indicated operation in the glow discharge regime even at nearly 10 atm, while spectroscopic measurements of the N_2 $C^3\Pi_u \rightarrow B^3\Pi_g$ emission returned rotational temperatures always around 420 K, with a pressure-dependent vibrational population distribution. The variation of breakdown voltage with pressure closely followed Paschen's law, but with offsets in both axes that we tentatively ascribe to strong diffusive loss and a partial thermalization of electron energies under the high pressures considered here.

Keywords: diamond, high pressure, glow discharge, microplasma

(Some figures may appear in colour only in the online journal)

1. Introduction

Hollow-cathode gas discharges are a technologically important class of non-equilibrium plasmas, which can support higher current densities than typical glow discharges between parallel-plate electrodes, while still exhibiting a pronounced population enhancement at the high end of the electron energy distribution relative to thermal arcs. The properties and behavior of these discharges have remained active research topics for over 50 years, and a wide variety of applications have been both proposed and realised. However, while many applications can benefit from high discharge powers, scaling is difficult in practice since low-pressure plasmas operating in the hollow-cathode regime still tend to become arcs as power density is further increased. One recognized approach to mitigating the glow-to-arc transition is the miniaturization of the discharge, as plasma sources with sub-millimetre dimensions afford the maintenance of stable, high-density nonthermal discharges in diverse working gases at pressures exceeding 1 atm [1].

'Microplasma' devices close the gulf between the archetypal low-pressure, cold discharge and the ambient environment and, in the space of little more than a decade, have been broadly adopted in scientific, medical, and industrial applications requiring energetic electrons or high densities of ions or reactive metastable/radical species. These include uses as high-efficiency sources of VUV excimer radiation [2, 3], for the remediation of environmental pollutants and destruction of biological pathogens [4], as ionization sources in mass spectrometers [5], for the detection of physical and chemical stimuli [6], in process chemistry [7], and as thrusters for space applications [8]. In many cases, however, material limitations constrain the usefulness of microdischarges: severe demands are placed on the electrodes by the high gas temperatures and ion energies produced under high-power, high-pressure dc operation, limiting the achievable power density and device lifetime.

Most microdischarge devices to date have employed electrodes manufactured either from Si, largely due to the availability of well-developed microfabrication techniques, or refractory metals such as Mo for their high melting points, good thermal and electrical conductivity, and low sputter yields. Advances in the growth of diamond by chemical vapour deposition (CVD) [9] have enabled the fabrication

of polycrystalline films on a variety of substrate materials (including patterned Si), with thicknesses ranging from less than 100 nm to many hundreds of microns. Thus, diamond can now be considered a practical and relatively inexpensive engineering material, and also a promising candidate for microdischarge applications due to its low sputter yield [10–12] and superlative thermal conductivity. The latter property is especially valuable in limiting the gas and cathode surface temperatures, thereby inhibiting thermionic emission and potentially enabling improved device lifetimes. Diamond is applicable to microplasma devices both in its undoped form as a high-dielectric-strength insulator (intrinsic/insulating diamond, ID) and also, when heavily boron-doped, as a low-resistivity, metallic [13] conductor suitable for use as a cathode material. This affords the possibility of monolithic, all-diamond substrates, thereby avoiding problems of thermal conductivity or expansion mismatch and manufacturing process incompatibility. So far, however, the use of boron-doped diamond (BDD) in this application has not received much attention, even despite its favourably low electron affinity and high secondary-electron yield in comparison to many metals. Indeed, Sakai *et al* have recently reported that the sustaining voltage for a macroscopic Ar glow discharge between planar BDD electrodes is about half that for Mo, and lower still when the BDD surface is hydrogenated [14].

The first, and so far only, demonstration of a monolithic diamond microdischarge device was that of Mitea *et al* [15], who employed a laser-milled cavity in a trilayer (BDD–ID–BDD) 'sandwich' (manufactured in our group) and described its operation at close to 0.5 atm in He. However, our subsequent experience has been that this design is fragile and difficult to operate at high pressure (due to the tendency for stable arcs to form, which then rapidly erode the thin BDD electrodes), while also proving complicated and time-consuming to manufacture. We report here on a new monolithic diamond device, chosen principally for its robustness and ease of fabrication, which demonstrates significant improvements in stability and longevity over those first attempts. In particular, we now discuss the much higher power densities, and pressures approaching 10 atm, to which the revised design affords routine access with good quantitative reproducibility. This harsh regime places special emphasis on the physical properties of the electrode material.

2. Experiments and methods

The devices investigated in this work were of a diamond bilayer (BDD hollow cathode–ID dielectric) design, as shown in figure 1. The cathode was formed of a commercial ≈ 600 μm thick, heavily boron-doped polycrystalline diamond plate (Element Six type PE), on one side of which a microcrystalline intrinsic diamond layer was grown by microwave-plasma-activated chemical vapour deposition (MWCVD). The dielectric layer thickness, $d \approx 50$ μm, was chosen as sufficient to ensure negligible grain-boundary conduction and to avoid breakdown in the presence of possible material inhomogeneities. An electron micrograph showing the two layers is given as figure 2, wherein the deposited ID appears bright due
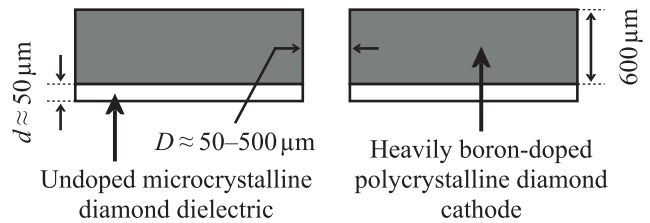

Figure 1. Cross-sectional schematic of the hollow-cathode microdischarge device tested in the present work.
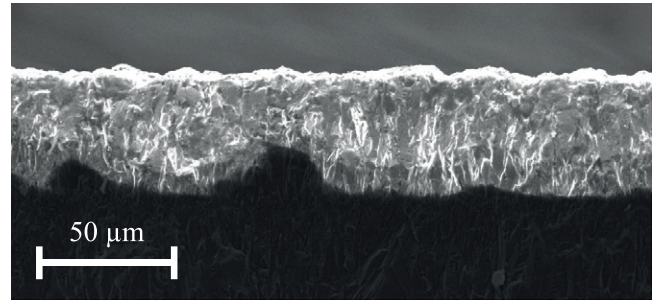

Figure 2. Scanning electron micrograph showing ≈ 50 μm-thick ID layer deposited by MWCVD (bright) on commercial BDD plate (dark).

to its high resistivity (leading to charging by the incident electron beam), whereas the conductive BDD substrate does not become charged, and so appears darker. The surface texture of the two layers appears similar, suggesting comparable crystallite sizes in both. Finally, a through hole of well-defined diameter in the range $50 \lesssim D \lesssim 500$ μm was laser-milled (Oxford Lasers Alpha 532 nm) for the discharge cavity, and the sample was washed in warm concentrated nitric acid to remove conductive (graphitic) surface residue.

For the (planar) anode, one end of a Mo rod was held in contact with the dielectric layer, centred on the through hole. Mo was employed here in place of BDD for practicality, since the behaviour of a glow discharge is typically quite insensitive to the anode material. The anode was connected to positive high voltage and, except for the face in contact with the diamond sample, completely encapsulated inside a Macor block such that a discharge could occur only within the device cavity. The exposed cathode was held at ground potential, and cathode and anode were each in contact with copper blocks, which both facilitated electrical connection and served as heat sinks in case of prolonged operation. The jig used to hold the devices for testing is depicted in figure 3.

Electrical characterization employed a high-voltage operational power supply (Kepco BOP 1000M, 1 kV/40 mA, $f_{-3\,\text{dB}} = 4.4$ kHz measured for a purely resistive load) operated as a rapidly variable dc current or voltage source (for current–voltage and breakdown measurements, respectively) and driven at typically 10 Hz with either a triangular or a sawtooth waveform. The latter were produced by a signal generator (Stanford Research DS340) and were preferred for their (piecewise) constant first derivatives, resulting in equally spaced abscissae when recorded at a constant sampling rate using an oscilloscope, although the results would not have been meaningfully altered for other reasonable choices of the test waveform.
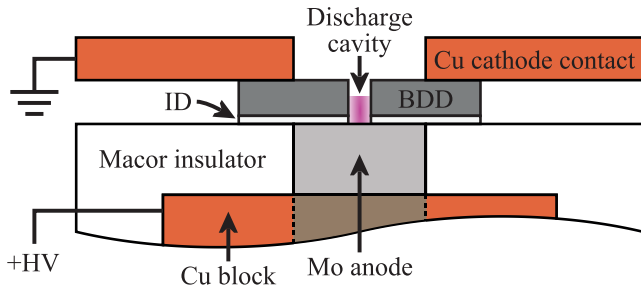
Figure 3. Schematic of the jig in which the microdischarge devices were held for testing, and which housed the Mo anode. (Anode and sample drawn larger than to scale for clarity.)

Table 1. Rotational and vibrational temperatures, and vibrational population difference ratios, measured for a ~1% N_2/He discharge in a device with $D = 200$ μm operating at $I = 8$ mA. Figures in parentheses represent one standard deviation in units of the last place. The uncertainties given for $\Delta N_{13}/\Delta N_{02}$ and $\Delta N_{24}/\Delta N_{13}$ do not incorporate contributions from the off-diagonal elements of the covariance matrix and are therefore approximate.

Pressure (atm)	T_{rot} (N_2) (K)	$\Delta N_{13}/\Delta N_{02}$	$\Delta N_{24}/\Delta N_{13}$	T_{vib} (N_2 $C^3\Pi_u$) (K)
0.5	397(8)	0.574(81)	0.314(99)	—
1.0	440(8)	0.456(50)	0.260(64)	—
2.0	381(8)	0.333(51)	0.302(104)	2540(17)
4.0	477(10)	0.258(31)	0.290(81)	2109(16)

Discharge voltage V and current I were measured with high-side (high voltage) and low-side voltage probes, plus a low-side current shunt ($R = 4.7$ kΩ), so that $V = V_{high} - V_{low}$ and $I = V_{low}/R$. The measurement bandwidth was dc to >10 MHz, with the wideband measurement being crucial in order to avoid misleading results in case of rapidly varying discharge characteristics. The raw *I–V* measurements sometimes exhibited random transient fluctuations (current spikes, etc), resulting in widely scattered points that tended to obscure the steady-state behaviour, so the data presented here represent (where appropriate, and solely for clarity of presentation) averages over typically 64 consecutive current ramps, with subsequent smoothing and temporal downsampling using a Savitzky–Golay filter. In all cases, care was taken to avoid introducing non-physical artefacts or obscuring any phenomena that were reproducibly observable in the real-time measurements.

Discharges were produced with the device sample and test jig contained within a pressure chamber (≈ 0.5 L volume) that was evacuated to <30 mbar using a diaphragm pump before being back-filled with He ($>99.996\%$). Helium was chosen as the discharge medium for its smaller atomic mass (thus limiting sputter damage to the diamond surface) and larger thermal conductivity (0.155 W m^{-1} K^{-1} at 25.0 °C and 1.0 atm [16]) than all other gases except for hydrogen, with the latter being unsuitable as H atoms are well known to etch diamond. After the removal of residual air by means of several initial evacuation/fill cycles, the chamber pressure was increased to the required value, up to a maximum of 10 atm, as measured by a piezoelectric manometer. A fused silica viewport permitted observation and spectroscopic measurements of the plasma using a fibre-coupled spectrograph that afforded spectral resolution (full width at half maximum, measured) of 0.15 nm in the near-UV.

3. Results and discussion

3.1. General observations

The diamond hollow-cathode devices operated reliably over wide ranges of pressure and discharge current, with a representative hole diameter $D = 200$ μm supporting stable discharges with glow-like *I–V* characteristics for $0.5 \leqslant p(\text{He}) \leqslant 7.0$ atm and $1 \leqslant I \leqslant 15$ mA. For $p(\text{He}) < 0.5$ atm, a diffuse corona- or brush-like discharge was present on the outer surface of the cathode in addition to that within the cathode cavity, with the former tending to become more filamentary with increasing I, although never transitioning to a stable arc. Owing to its small dimensions and rapidly varying structure, we were not able to study the surface discharge in detail in the present work. However, the fact of its appearance leads us to suspect that much of the transient fluctuation observed in other cases (elaborated further below) was due to streamer formation inside the cavity, which nonetheless could not be observed directly.

The sustaining voltage generally increased with pressure, but remained close to 250 V under all conditions, so that total discharge powers were approximately ¼–4 W, depending on current. Accurate determination of either the plasma volume or the effective cathode area was not possible due to the combination of the small size of the discharge and the experimental geometry, and therefore we do not report power or current densities. However, a modelling study by Kothnur and Raja [17] calculated the peak power density near the cathode surface to exceed 100 kW cm^{-3} for a 0.5 mA discharge in 1000 Torr He occurring within a 200 μm cavity, and these conditions clearly lie at the low end of our experimental regime.

Gas temperature was estimated, after the addition of ~1% N_2 to the He working gas, from the rotational contour of the $\Delta v = -2$ progression of the N_2 $C^3\Pi_u \rightarrow B^3\Pi_g$ (second positive system) emission spectrum in the range 368–382 nm. Analysis was conducted using Western's PGOPHER software [18], with spectroscopic constants as given by Roux *et al* [19] and transition probabilities according to Gilmore *et al* [20]. The experimental spectra and corresponding simulations are provided as PGOPHER files in the supplementary and supporting information (available at http://dx.doi.org/10.5523/bris.vnf7pv0gg4av1wri2845bual7). An average rotational temperature, $T_{rot}(N_2) \triangleq T_{gas}$ [21], was found as 419(31) K for a device with $D = 200$ μm operating at $I = 8$ mA; $T_{rot}(N_2)$ was essentially independent of pressure, as shown in table 1. Vibrational temperatures, $T_{vib}(N_2\ C^3\Pi_u)$, were assessed for the two highest pressures from the relative band intensities under approximation to Maxwellian $C^3\Pi_u$-state vibrational populations, and these are also given in table 1. Here, the $B^3\Pi_g$-state populations were taken to be negligible, since accounting for self-absorption by setting $T_{vib}(N_2\ B^3\Pi_g) = T_{vib}(N_2\ C^3\Pi_u)$ in the simulation yielded a poorer fit to the measured spectra. In the other cases, due to strongly non-equilibrium observed intensities, only the band-to-band population difference ratios

$\Delta N_{v-1,v+1}/\Delta N_{v-2,v}$ are given, where e.g. $\Delta N_{v-2,v} = N(N_2$ $C^3\Pi_u, v-2) - N(N_2 B^3\Pi_u, v)$. Clearly, $T_{vib}(N_2 C^3\Pi_u)$ is considerably greater than $T_{rot}(N_2)$ for both applicable pressures, which seems encouraging in respect of possible chemical processing applications of these plasmas.

Emission spectra measured after nitrogen addition also revealed structure due to the $B^2\Sigma_u^+ \rightarrow X^2\Sigma_g^+$ (first negative) system of N_2^+, the $\Delta v = +1$ progression of which overlapped the N_2 $C^3\Pi_u \rightarrow B^3\Pi_g$ $\Delta v = -1$ bands between 347 and 360 nm. The ionization energy of N_2 is 15.58 eV [22] and the $N_2^+ B^2\Sigma_u^+$-state $v = 0$ energy (relative to the $X^2\Sigma_g^+$ $v = 0$ ground state) is 3.17 eV [23], as compared with the N_2 $C^3\Pi_u$-state $v = 0$ energy of 12.10 eV [24]. The ionization fraction did not appear to vary significantly with pressure, as judged by the almost constant relative intensities of the N_2 and N_2^+ emissions. However, it was not possible to determine an electron temperature spectroscopically. Boltzmann analysis applied to He [25] and Ne [26] lines (from 1:1 He/Ne discharges, in the latter case) both yielded excitation temperatures $T_{exc} \approx 0.3$ eV, which is an unphysical but typical result for atmospheric-pressure He discharges owing to an inefficient exchange of energy between electronic states coupled with a high rate of diffusive loss [27, 28]. While the same outcome for Ne would seem at first less plausible because of the greater mass of the atoms and the rather small separations in energy between the upper states of the observed lines, the discharge dimensions in the present case are such that diffusion may still dominate regardless. The problem is exacerbated by the sampling of only a small range of excited state energies (23.0–23.7 and 18.6–18.7 eV, respectively, for the visible He and Ne lines), and in fact a comparable result has been reported previously [29] for a (low-pressure) Ne hollow-cathode discharge. Given the strongly non-Maxwellian electron energy distribution function (EEDF) distinguishing glow discharges, with a significant minority of electrons gaining energies extending up to the cathode fall potential [30, 31], any (Maxwellian) temperature derived from transitions between high-lying excited states should clearly be viewed with suspicion. Further rovibronic transitions were observed in the region 382–392 nm that could be assigned as the overlapping $\Delta v = 0$ progressions of $N_2^+(B^2\Sigma_u^+ \rightarrow X^2\Sigma_g^+)$ and $CN(B^2\Sigma^+ \rightarrow X^2\Sigma^+)$, with the latter possibly indicative of reactive etching in the presence of nitrogen.

Comparable discharges in Ne and Ar exhibited current waveforms dominated by short, intense spikes suggestive of streamers or unstable arcs. The lower ionization probability in gases with larger Stoletov constants (100 V cm^{-1} Torr^{-1} for Ne and 200 V cm^{-1} Torr^{-1} for Ar, versus 50 V cm^{-1} Torr^{-1} for He [32]) should, however, disfavour the glow-to-arc transition, and thus the repetitive increase in current density relative to the stable glow is unlikely to be a spontaneous instability but rather initiated by some process peculiar to the heavier working gases. Since these discharges possessed unsteady current–voltage (I–V) characteristics that tended toward a short-circuit failure mode, the observations are consistent with sputtering of the diamond cathode under Ne$^+$/Ar$^+$ bombardment, accompanied by intense secondary-electron
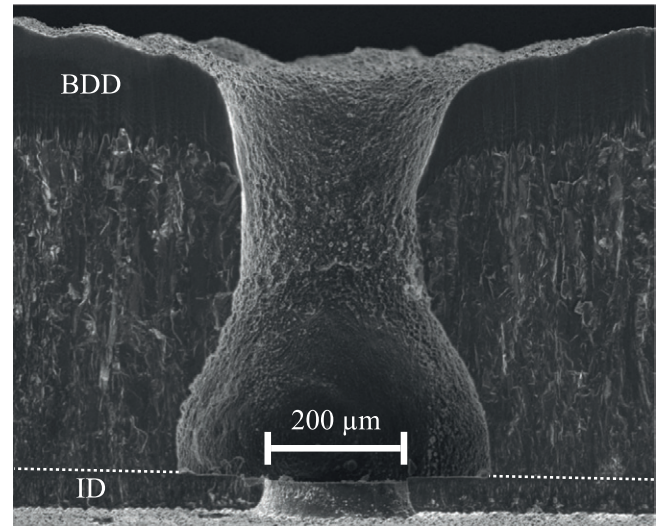

Figure 4. Scanning electron micrograph of a bisected microdischarge device, showing cross-section of eroded cathode (original hole diameter $D = 200$ μm) and unaffected dielectric layer after $\approx$5 h continuous operation at $\approx$1 W discharge power under $p(\text{He}) = 3$ atm.
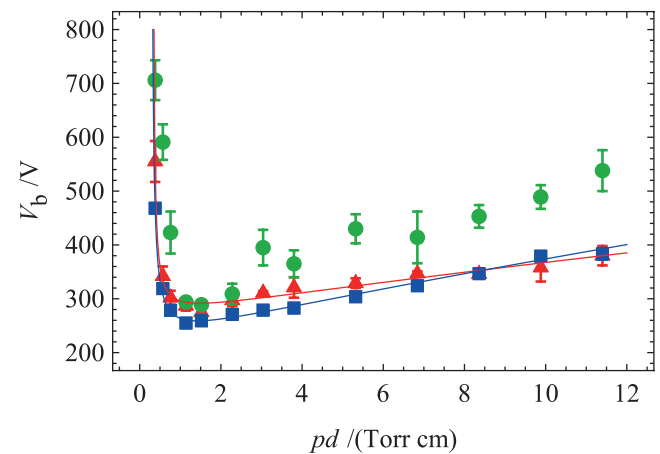

Figure 5. V_b (breakdown voltage) versus pd (the product of the pressure and the anode–cathode separation) plotted for three devices with different cavity geometries. Key: red triangles, $D = 300$ μm; green circles, $D = 200$ μm; blue squares, 0.2×1.0 mm rectangular slit. The solid lines are fits to equation (1), with parameters as given in table 2.

emission. Erosion of the cavity interior, and carbon redeposition as porous graphite within the blind hole, can hence be understood as responsible for the time-dependent I–V curves and eventual device failure.

In He, the discharge properties remained qualitatively stable for >30 min, indicating little dimensional change on this timescale, which is consistent with a lower sputter yield for He$^+$. The cumulative sputter damage after operation for a prolonged period is shown in figure 4, which depicts a device operated continuously at high power density until an ohmic characteristic was obtained. The damage mechanism is clearly non-thermal given that the erosion is concentrated on that part of the cathode lying closest to the anode, producing a bulbous cavity while leaving the dielectric layer unaffected.

Table 2. Best-fit values of the Paschen parameters and required pd and V_b offsets for the breakdown curves given in figure 5. Figures in parentheses represent one standard deviation given in units of the last place.

Cavity geometry (with $d \approx 50\ \mu$m)	A (Torr^{-1} cm^{-1})	B (V Torr^{-1} cm^{-1})	γ	pd offset (Torr cm)	V_b offset (V)
$D = 200\ \mu$m	3.624(0)	110(1)	0.053(21)	$-0.59(1)$	72(5)
$D = 300\ \mu$m	2.480(10)	39(4)	0.229(50)	$-0.36(9)$	220(15)
0.2×1.0 mm slit	2.472(3)	58(1)	0.240(15)	$-0.39(3)$	153(5)

3.2. Breakdown voltages

Breakdown experiments were conducted for a voltage ramp rate such that repeated breakdowns occurred consistently at a particular applied field. In practice, a rate of ~100 V s^{-1} was sufficiently small for this condition to be fulfilled. Measured breakdown curves, shown in figure 5 for three different cavity geometries, closely resembled those of a Townsend discharge between parallel-plate electrodes. Furthermore, although no well-defined parallel-plate-equivalent cathode–anode separation exists in the present case, putting $d = 50\ \mu$m (corresponding to the approximate thickness of the dielectric layer) yielded good agreement with the classical Paschen relationship, i.e.

$$V_b = \frac{Bpd}{\ln(Apd) - \ln[\ln(1 + 1/\gamma)]} \tag{1}$$

with close-to-typical [33] values of the parameters A, B, and γ (given in table 2) after applying offsets in both the pd and V_b axes. The physical interpretation of the shifted Paschen curve and its parameters is less certain, however, particularly given that A and γ (as determined by least-squares fitting) are strongly correlated both with each other and the empirical offsets, making the proper values somewhat unclear. While (low-pressure, macroscopic) hollow-cathode discharges are well-known to exhibit breakdown curves with minima lying to lower pd than parallel-plate glow discharges, their minimum V_b is generally also reduced [34], which is in fact a similar situation to that of a parallel-plate discharge inside a cylindrical tube if the electrode spacing is small relative to the tube diameter. As noted by Lisovskiy and Yakovin [35] for the latter scenario, this can seemingly only be due to the varying influence of diffusive wall losses, and can be accommodated while retaining the classical relation by scaling the axes by a factor of the form

$$u = \left[1 + \left(\frac{d}{r}\right)^2\right]^{-\chi} \tag{2}$$

where r is the electrode radius and χ depends on the working gas. However, such a scaling (of either axis) cannot adequately reproduce the present measurements, suggesting a further departure from the parallel-plate case.

The close correspondence among the breakdown curves for all three geometries, with minima of V_b at $pd \approx 1.5$ Torr cm ($p \approx 300$ Torr), suggests that breakdown occurs along short, direct paths between the cathode and anode and with minimal effect due to electric field non-uniformity within the cavity. That this occurs at a larger voltage than in a parallel-plate discharge is hence probably due to a more nearly thermal EEDF

under these highly collisional conditions, i.e. with little or no contribution from those electrons unable to produce an avalanche before being rethermalized and/or lost to the walls. The pd shift can be understood similarly: since almost all electrons will suffer multiple collisions, the distance over which thermalization occurs, and thus the effective value of d, may be somewhat less than the geometrical value. However, this does not entirely exclude long-path breakdown, which could also contribute to the observed offsets at low pressures for which diffusive losses do not yet dominate [36]. The shift of the minimum of V_b to smaller pd for the hollow-cathode geometry can be understood in this case as resulting from the superimposition of breakdown curves for a range of effective values of d, between the minimum possible and that for which E/N at some point along the ionization path becomes small enough that loss processes on average overwhelm any energy gain.

It is worth noting that the measurements for the device with $D = 200\ \mu$m were not well modelled by the shifted form of (1), and could be reproduced only with A and B very large and γ very small. The smaller D is likely to both increase diffusive electron losses, especially at the higher pressures for which the relative increase in V_b is most evident, and diminish the significance of long-path breakdown. Additionally, it was difficult to produce well-formed holes with small diameters in the relatively thick diamond samples, and so the actual geometry of this device may not have been as close to ideal as for the other two, which could further increase the loss probability. Empirically, however, figure 5 illustrates at most a small dependence of the breakdown curve on the cavity dimensions, which is in agreement with the finding of Sismanoglu and Amorim [37] that the breakdown curve did not vary over a wide range of D for a low-aspect-ratio hollow-cathode microdischarge.

3.3. Current–voltage characteristics

Current–voltage (I–V) characteristics were almost flat for all p(He) $\geqslant 1$ atm, regardless of cavity dimensions, with typical sustaining voltages of $220 < V < 320$ V over the range $I = 3$–15 mA. For small I and at p(He) > 2 atm, the discharges tended to possess unstable (self-oscillating) I–V relationships, while the regime $I > 15$ mA was not investigated because there was no evidence for greatly different behaviour at large I. Overall, our observations strongly resembled those reported by Schoenbach *et al* [31] for hollow-cathode Ar microdischarges, although extending to rather higher pressure.

A representative I–V plot, showing one period of a triangular current waveform lasting 1 s, is given in figure 6 for a device with $D = 100\ \mu$m operating at p(He) = 3.0 atm.
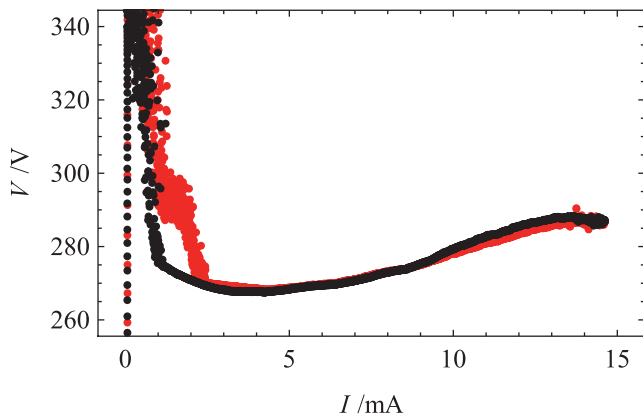
Figure 6. Typical *I*–*V* characteristic for a device with $D = 100$ μm operating under p(He) $= 3.0$ atm. Red points are drawn for the upward current ramp, and black points for the downward ramp.

While the portions of the curve measured for increasing and decreasing current almost coincide, they are not identical; in particular, the unstable range (scattered points) extends to $I \approx 2$ mA on the upward ramp, but only occurs for $I \lesssim 1$ mA on the downward ramp. The narrow, intense, and regular current pulses observed for the unstable discharge were characteristically relaxation oscillations, which have been widely reported and latterly comprehensively described by Aubert *et al* [38]. However, the nature of the relaxation process may differ depending on the circumstances. Given the filamentary structures observed on the cathode outer surface at low pressure and the unpredictable transient current spikes noted in the *I*–*V* characteristics, we consider streamer formation to be the most probable mechanism in the present case, consistent with the early report of Schoenbach *et al* [31]. The greater instability with respect to oscillation during breakdown into a self-sustaining glow, as compared to when the same discharge is being extinguished, most likely reflects a dependence of the streamer formation probability on cathode surface condition.

In general, sustaining voltages were smaller for *I* falling than rising, which was observed even with rather slowly varying current well above the breakdown range. (Large current slew rates were avoided because of the possibility of ac conduction through the poorly characterized sheath capacitance.) This hysteresis hence probably resulted also from changes to the diamond surface (e.g. reconstruction or graphitization) on exposure to He plasma, which can significantly alter its secondary-electron yield.

For p(He) $\leqslant 1$ atm, a region of strongly positive differential resistance (diagnostic of a Townsend discharge) was observed instead of self-oscillation for small *I*, as shown in figure 7. With progressively increasing current, an abrupt transition occurred that was characterized by a sharp fall in sustaining voltage followed by a second, milder increase. Such behaviour is symptomatic of the unconfined normal glow regime, with expansion of the discharge out of the cavity and onto the outer surface of the cathode. This structure of hollow cathode microdischarges at intermediate pressures has been described both for the present geometry and working gas in the work of Kothnur and Raja [17] and, in more detail but for different experimental parameters, in the more recent studies by Lazzaroni, Chabert, and co-workers
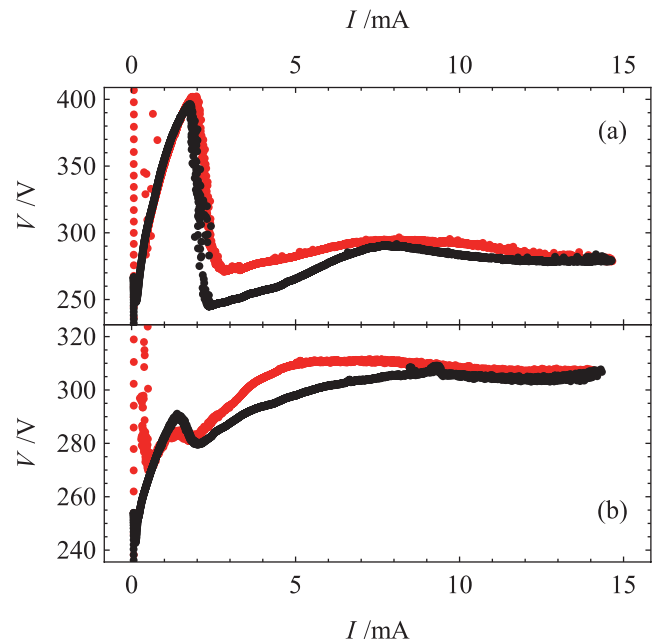

Figure 7. *I*–*V* characteristics for a device with $D = 100$ μm operating under (a) p(He) $= 0.5$ atm and (b) 1.0 atm, showing low-pressure positive differential resistance regime at small *I*. In each case, red points are drawn for the upward current ramp, and black for the downward ramp.

[39, 40]. We also observed the Townsend and 'expansionary' normal modes for a cavity of $D = 200$ μm under p(He) $= 0.5$ atm, which in that case continued to exhibit (smaller) negative differential resistance even as *I* was further increased, indicating more extensive coverage of the back side of the cathode. Conversely, these distinct low-current modes were much less clear for $D \approx 50$ μm/p(He) $= 1.0$ atm, suggesting hindered expansion for small cavities, and absent altogether at higher pressures. The *I*–*V* characteristics in the transitional pressure range, e.g. that of figure 7(b), bear some similarity with the gentle positive slope predicted in the previous work [17], but with a rather higher sustaining voltage and strong *D*-dependence in their detailed form (see supplementary and supporting information http://dx.doi.org/10.5523/bris. vnf7pv0gg4av1wri2845bual7).

With further increasing pressure, the minimum of sustaining voltage first moved to higher *I* and thereafter increased in absolute value, and the inflected *I*–*V* characteristic of figure 6 became uniformly downward sloping. Figure 8 shows the operation of the device with $D = 100$ μm for $3.0 \leqslant p$(He) $\leqslant 8.0$ atm, where the smooth progression suggests the applicability of consistent physical principles over this range. Equivalent (although less picturesque) results were obtained for devices having $D = 50$, 200, and 300 μm, and pD and I/D scaling relations appeared to apply, at least approximately, to the evolution of the *I*–*V* curves with respect to pressure and current. At high pressure, the discharge is known to become localized within the cavity, and power is dissipated predominantly in the cathode sheath, producing an annular structure. Furthermore, the sheath width, which can be some tens of microns (depending on the secondary-electron yield for ion impact on the cathode) close to 0.5 atm, decreases
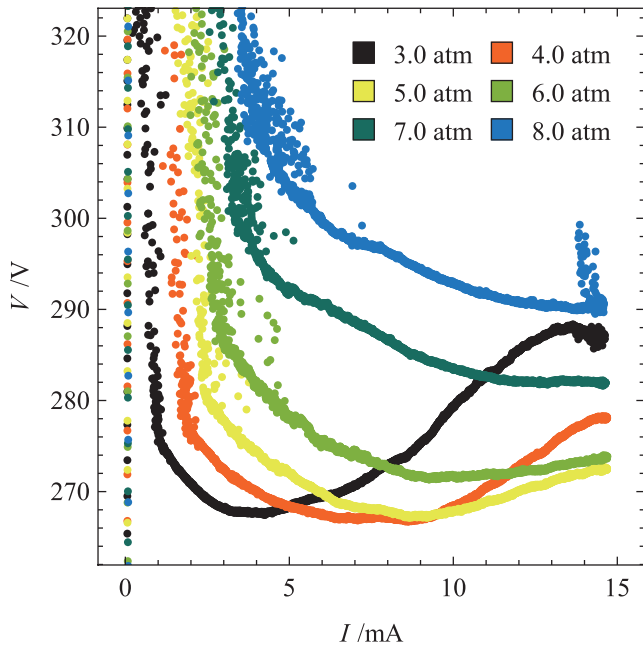
Figure 8. *I–V* characteristics for a device with $D = 100\ \mu m$ operating under $3.0 \leqslant p(\mathrm{He}) \leqslant 8.0$ atm. For clarity, only the (smoother) curves for falling I are shown.

strongly with increasing p [17, 39, 40]. Lazzaroni *et al* have shown that a non-ionizing (strongly collisional) sheath model fails to reproduce experimental measurements, and so the increase of sustaining voltage cannot be understood as due to a reduced ion–neutral mean free path within a relatively thick sheath. Rather, it would seem that a greater surface-to-volume ratio for the discharge leads to a strong influence of diffusive losses, at least in He, and that the local reduced electric field (which falls rapidly with distance from the anode) limits the extent of cathode coverage. We thus have a confined normal glow with an almost flat, loss-dominated *I–V* characteristic; the small negative gradient corresponds, as in the usual case, to the expansion of the discharge over the cathode surface at constant current density. 'Complete' coverage, and thus the abnormal glow mode, is possible only for rather high discharge currents at intermediate pressures of not more than several atmospheres. Increasing $p(\mathrm{He})$ has the effect of reducing the discharge volume and increasing current density, which causes a corresponding increase in sustaining voltage. The scalings with D can then be accounted for according to the cathode surface area available to a discharge of given volume in differently sized cavities.

Glow discharges at $p(\mathrm{He}) \gtrsim 9$ atm could be produced only within the smallest cavities, $D \approx 50\ \mu m$ or $D = 100\ \mu m$, and at relatively high currents, $I \gtrsim 5$ mA. Stable operation at the highest pressure investigated, $p(\mathrm{He}) = 9.5$ atm, was achieved only for $D \approx 50\ \mu m$, and such a discharge was maintained, with a sustaining voltage of approximately 320 V, for ≈ 30 min before the device failed due to sputtering damage.

The 0.2×1.0 mm slit cavity demonstrated an exceptionally flat *I–V* characteristic ($V = 285 \pm 5$ V over the range $0.5 \leqslant I \leqslant 15$ mA) under $p(\mathrm{He}) = 2.0$ atm, and the discharge could be seen to occupy a changing proportion of the cavity

volume as I was varied. The essentially constant V thus indicated operation in an extended normal glow regime, which was approximately reproduced also for $p(\mathrm{He}) = 1.0$ and 3.0 atm. However, the discharge became progressively more localized for $p(\mathrm{He}) \geqslant 4.0$ atm, under which conditions the sustaining voltage was markedly reduced ($220 < V < 240$ V). This is in obvious contrast to the situation for the cylindrical cavities, and was apparently due to an increasingly arc-like character of the discharge owing to diminished wall losses for this particular geometry.

4. Conclusions

In this work, we have demonstrated high-pressure, high-power-density non-equilibrium glow discharges in monolithic diamond hollow-cathode devices, with ≈ 30 min continuous operation at 9.5 atm being achieved for the smallest cavity, $D \approx 50\ \mu m$. The maximum $p(\mathrm{He})$ was limited by the capacity of our pressure chamber to withstand it, while the device lifetime was constrained by sputtering of the diamond cathode surface, which both eroded the cavity interior and produced graphitic residue that tended to block the hole and short-circuit the anode and cathode. In practice, the short-circuit failure mode was exacerbated by the construction of the cavity as a blind hole, and could be ameliorated in other geometries. A useful device lifetime (i.e. within which quantitatively reproducible measurements could be obtained) of at least several hours was typical for less extreme conditions of $p(\mathrm{He}) \approx 3$ atm and with larger $D > 100\ \mu m$ due to the reduced relative impact of sputtering damage. Such pressures are already among the highest reported for stable non-thermal discharges, which would tend to suggest that diamond is indeed a promising microdischarge electrode material.

Breakdown proceeded by electron avalanche, and depended only weakly on cavity geometry, but occurred at significantly higher voltage than would be expected according to Paschen's law (owing, in our view, to strong diffusive loss) and slightly smaller values of the *pd* product (most likely due to electron thermalization, with a smaller but potentially still non-negligible contribution from long-path breakdown). Low-pressure ($\leqslant 1$ atm) *I–V* characteristics indicated operation in the Townsend regime, with discharge expansion onto the cathode outer surface with increasing I, whereas only 'confined normal' and abnormal glow modes were apparent for $p(\mathrm{He}) \geqslant 2.0$ atm. Spectroscopic determinations of the gas temperature yielded values around 420 K, irrespective of pressure.

Supplementary information

Data used in the preparation of this paper are available from the University of Bristol research data repository under DOI 10.5523/bris.vnf7pv0gg4av1wri2845bual7. Experimental measurements are also included for those devices and conditions referenced but not presented in detail here.

References

[1] Becker K H, Schoenbach K H and Eden J G 2006 Microplasmas and applications *J. Phys. D: Appl. Phys.* **39** R55–70

[2] Moselhy M, Petzenhauser I, Frank K and Schoenbach K H 2003 Excimer emission from microhollow cathode argon discharges *J. Phys. D: Appl. Phys.* **36** 2922–7

[3] Kurunczi P, Lopez J, Shah H and Becker K 2001 Excimer formation in high-pressure microhollow cathode discharge plasmas in helium initiated by low-energy electron collisions *Int. J. Mass Spectrom.* **205** 277–83

[4] Becker K, Koutsospyros A, Yin S-M, Christodoulatos C, Abramzon N, Joaquin J C and Brelles-Mariño G 2005 Environmental and biological applications of microplasmas *Plasma Phys. Control. Fusion* **47** B513–23

[5] Li W, Yin Z, Cheng X, Hang W, Li J and Huang B 2015 Pulsed microdischarge with inductively coupled plasma mass spectrometry for elemental analysis on solid metal samples *Anal. Chem.* **87** 4871–8

[6] Eun C K and Gianchandani Y B 2012 Microdischarge-based sensors and actuators for portable microsystems: selected examples *IEEE J. Quantum Electron.* **48** 814–26

[7] Taylan O and Berberoglu H 2015 Dissociation of carbon dioxide using a microhollow cathode discharge plasma reactor: effects of applied voltage, flow rate and concentration *Plasma Sources Sci. Technol.* **24** 015006

[8] KC U, Deconinck T, Varghese P L and Raja L L 2011 Experimental and numerical studies of a direct current microdischarge plasma thruster *Prog. Propuls. Phys.* **2** 585–600

[9] May P W 2000 Diamond thin films: a 21st-century material *Phil. Trans. R. Soc.* A **358** 473–95

[10] De Temmerman G *et al* 2009 Interactions of diamond surfaces with fusion relevant plasmas *Phys. Scr.* **T138** 014013

[11] Dunn A 2011 A molecular dynamics study of diamond as a plasma facing material for fusion *PhD Thesis* University College London Available: http://discovery.ucl.ac.uk/1136851/

[12] Blandino J J, Goodwin D G and Garner C E 2000 Low energy sputter yields for diamond, carbon–carbon composite, and molybdenum subject to xenon ion bombardment *Diam. Relat. Mater.* **9** 1992–2001

[13] Yokoya T, Nakamura T, Matsushita T, Muro T, Takano Y, Nagao M, Takenouchi T, Kawarada H and Oguchi T 2005 Origin of the metallic properties of heavily boron-doped superconducting diamond *Nature* **438** 647–50

[14] Sakai T, Ono T, Sakuma N, Yoshida H, Suzuki M, Takeuchi D, Kono S and Yamasaki S 2014 Observation of negative electron affinity in low-voltage discharging boron-doped polycrystalline diamond *Jpn. J. Appl. Phys.* **53** 05FP09

[15] Mitea S, Zeleznik M, Bowden M D, May P W, Fox N A, Hart J N, Fowler C, Stevens R and Braithwaite N St J

[16] Bich E, Millat J and Vogel E 1990 The viscosity and thermal conductivity of pure monatomic gases from their normal boiling point up to 5000 K in the limit of zero density and at 0.101325 MPa *J. Phys. Chem. Ref. Data* **19** 1289–305

[17] Kothnur P S and Raja L L 2005 Two-dimensional simulation of a direct-current microhollow cathode discharge *J. Appl. Phys.* **97** 043305

[18] Western C M 2014 PGOPHER, a program for simulating rotational structure version 8.0 (University of Bristol) Available: http://pgopher.chm.bris.ac.uk/

[19] Roux F, Michaud F and Vervloet M 1993 High-resolution Fourier spectrometry of $^{14}N_2$ violet emission spectrum: extensive analysis of the $C^3\Pi_u \to B^3\Pi_g$ system *J. Mol. Spectrosc.* **158** 270–7

[20] Gilmore F R, Laher R R and Espy P J 1992 Franck-Condon factors, *r*-centroids, electronic transition moments, and Einstein coefficients for many nitrogen and oxygen band systems *J. Phys. Chem. Ref. Data* **21** 1005–107

[21] Bruggeman P J, Sadeghi N, Schram D C and Linss V 2014 Gas temperature determination from rotational lines in non-equilibrium plasmas: a review *Plasma Sources Sci. Technol.* **23** 023001

[22] Trickl T, Cromwell E F, Lee Y T and Hung A H 1989 State-selective ionization of nitrogen in the $X^2\Sigma_g^+$ $v_+ = 0$ and $v_+ = 1$ states by two-color (1 + 1) photon excitation near threshold *J. Chem. Phys.* **91** 6006–12

[23] Klynning L and Pagès P 1982 The band spectrum of N_2^+ *Phys. Scripta* **25** 543–60

[24] Lofthus A and Krupenie P H 1977 The spectrum of molecular nitrogen *J. Phys. Chem. Ref. Data* **6** 113–307

[25] Weise W L and Fuhr J R 2009 Accurate atomic transition probabilities for hydrogen, helium, and lithium *J. Phys. Chem. Ref. Data* **38** 565–719

[26] Weise W L, Smith M W and Glennon B M 1966 Atomic transition probabilities, vol. I: hydrogen through neon *Natl. Stand. Ref. Data Ser.—Natl. Bur. Stand.* **4** (Washington, DC: National Bureau of Standards) Available: http://nist.gov/data/nsrds/NSRDS-NBS4.pdf

[27] Jonkers J and Van der Mullen J A M 1999 The excitation temperature in (helium) plasmas *J. Quant. Spectrosc. Radiat. Transfer* **61** 703–9

[28] Jonkers J, Van de Sande M, Sola A, Gamero A and Van der Mullen J 2003 On the differences between ionizing helium and argon plasmas at atmospheric pressure *Plasma Sources Sci. Technol.* **12** 30–8

[29] Mahmood S, Shaikh Nek M, Kalyar M A, Rafiq M, Piracha N K and Baig M A 2009 Measurements of electron density, temperature and photoionization cross sections of the excited states of neon in a discharge plasma *J. Quant. Spectrosc. Radiat. Transfer* **110** 1840–50

[30] Martín-Rojo A B, Oyarzabal E and Tabarés F L 2013 Characterization of suprathermal electron population in He dc glow discharges by optical emission and probe diagnostics *Plasma Sources Sci. Technol.* **22** 035001

[31] Schoenbach K H, El-Habachi A, Shi W and Ciocca M 1997 High-pressure hollow cathode discharges *Plasma Sources Sci. Technol.* **6** 468–77

[32] Yakovlenko S I 2007 Optimum conditions of the runaway electron beam generation during a uniform gas breakdown *Bull. Lebedev Phys. Inst.* **34** 61–5

[33] Burm K T A L 2007 Calculation of the Townsend discharge coefficients and the Paschen curve coefficients *Contrib. Plasma Phys.* **47** 177–82

[34] Eichhorn H, Schoenbach K H and Tessnow T 1993 Paschen's law for a hollow cathode discharge *Appl. Phys. Lett.* **63** 2481–3

[15] Mitea S, Zeleznik M, Bowden M D, May P W, Fox N A, Hart J N, Fowler C, Stevens R and Braithwaite N St J 2012 Generation of microdischarges in diamond substrates *Plasma Sources Sci. Technol.* **21** 022001

[35] Lisovsky V A and Yakovin S D 2000 Scaling law for a low-pressure gas breakdown in a homogeneous DC electric field *JETP Lett.* **72** 34–7

[36] Marić D, Škoro N, Maguire P D, Mahony C M O, Malović G and Petrović Z Lj 2012 On the possibility of long path breakdown affecting the Paschen curves for microdischarges *Plasma Sources Sci. Technol.* **21** 035016

[37] Sismanoglu B N and Amorim J 2008 Microhollow cathode discharge and breakdown in micron separations *Eur. Phys. J. Appl. Phys.* **41** 165–72

[38] Aubert X, Bauville G, Guillon J, Lacour B, Puech V and Rousseau A 2007 Analysis of the self-pulsing operating mode of a microdischarge *Plasma Sources Sci. Technol.* **16** 23–32

[39] Lazzaroni C, Chabert P, Rousseau A and Sadeghi N 2010 The excitation structure in a micro-hollow cathode discharge in the normal regime at medium argon pressure *J. Phys. D: Appl. Phys.* **43** 124008

[40] Lazzaroni C and Chabert P 2011 A global model of micro-hollow cathode discharges in the stationary regime *J. Phys. D: Appl. Phys.* **44** 445202